Progress In Electromagnetics Research, PIER 48, 301–333, 2004

PULSE COMPRESSION USING A PERIODICALLY DIELECTRIC LOADED DISPERSIVE WAVEGUIDE

E. C. Thirios, D. I. Kaklamani, and N. K. Uzunoglu

School of Electrical and Computer Engineering
National Technical University of Athens
9, Iroon Polytechniou Str., 157 73 Zografou, Athens, Greece

Abstract—The study of periodically dielectric-slab-loaded TE_{10} waveguide structures of conductive walls and finite length is carried out by using wave analysis techniques. The principal aim is to design and construct a highly dispersive waveguide keeping losses to a minimum. Passing a properly frequency modulated wave through this waveguide, pulse compression phenomena take place. Frequency modulated waves, incident to a finite length periodic loaded waveguide, are studied. The aim is to achieve optimum pulse compression, by taking into account all wave phenomena involved. In order to minimize the reflected (at the input) and maximize the transmitted (at the output) waves of the compressor structure, a staggered-tapered structure of dielectric slabs inside the waveguide is utilized to match the incident waves. The slab longitudinal discontinuity nature prevents the appearance of field singularity points that could hinder the operation of the compression mechanism. An exact Fourier analysis is carried out to compute the compressed wave field intensities. Optimization techniques are used to achieve the best compression and matching conditions for various realistic dielectric materials, having permittivities ε_r in the range of 9 to 36 and loss factors $\tan(\delta)$ in the range of 0.01 to 0.00001. Experimental results, obtained by carrying out measurements on prototype waveguide structures, built in our laboratory, present pulse compression phenomena, but do not show good agreement with theory.

1. INTRODUCTION

The concept of pulse compression in radar receivers was developed in the early 1950's in an attempt to increase the range. During the period 1940–1950 the research was focused on the increase of transmitter peak power. Then it was discovered that many of practical and physical factors restricted power amplification. Those were overcome by the pulse compression phenomenon in the receiver radar using highly dispersive circuits at intermediate frequency band.

During the last decades, high power RF systems have been developed and tested to achieve pulse compression phenomena for the enhancement of peak power levels. In the work of Tantawi et al. [1], the Stanford Linear Energy Development II (SLED II) [2] system of compression is presented. The SLED II is relied on an optically controlled high-power RF pulse compression system, which is based on the switched resonant delay-line theory [2]. Another important structure is the binary pulse compression (BPC) [3] system, which is also based on the use of delay line theory.

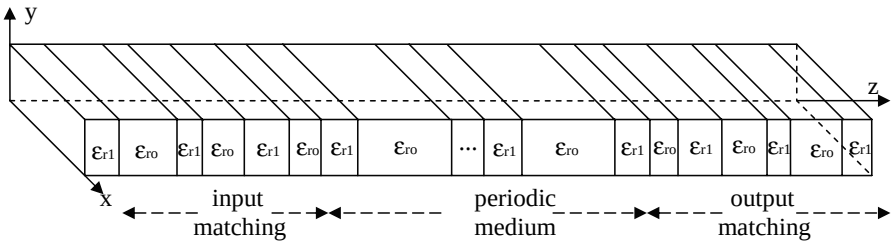

Figure 1. Periodically loaded waveguide structure with matching transformers.

The fundamental mechanism, used in the present paper to achieve compression, is the passing of a frequency modulated incident wave through a dispersive waveguide section satisfying pulse compression conditions. The proposed technique has the uniqueness of trying to achieve dispersive compression at high power level by using a passive medium in the microwave spectrum. The proposed dispersive structure, shown in Fig. 1, consists of a periodically loaded waveguide. The metallic wall waveguide is of type WR-340. The periodic structure is composed of rectangular layers with alternating relative dielectric permittivities of ε_{ro} and ε_{r1}. Their width and height are the same with the internal dimensions of the waveguide. At the input and output of the periodic medium, identical matching transformers are positioned, consisting of a finite number of non-periodic layers, as also shown in Fig. 1. The structure on both sides, is considered to be connected to an empty infinite length waveguide. This arrangement acts as a perfect mirror for some spectral frequency regions and as a band pass filter by some others. A good theoretical analysis of a one-dimensional periodic medium is presented in [4]. Also pulse propagation in dispersive media is studied in [5].

In Section 2, the guiding structure analysis is introduced, in order to determine the position, the magnitude and the form of the pulse compression phenomenon. In Section 3, the numerical computations of the propagation characteristics for different dispersive mediums and computations of pulse compression are presented. Furthermore, inclusion of metallic wall losses was also taken into account and proved to be insignificant for the case of copper waveguides. Finally, in Section 4, experimental study of a dispersive medium of 14 unit cells is carried out.

2. ANALYSIS OF THE GUIDING STRUCTURE

2.1. Analysis of the Finite Structure

The analysis of the finite length periodic structure, as defined in Fig. 1, can be analyzed by considering the standing waves in each layer of the structure while in case that $z \to +\infty$ and $z \to -\infty$ then only transmitted and reflected waves are taken into account.

The proposed periodic structures present successive discontinuities, which are perpendicular to the direction of propagation. No coupling occurs between the TE and TM modes. Consequently, if, initially, only the dominant mode TE_{10} is excited, it will be the only one that will propagate across the periodic waveguide. An incident TE_{10} mode originating at $z \to -\infty$ is considered. The TE_{10} mode field distribution in each layer of a finite periodic structure has the following form,

$$E_y = \sin\left(\frac{\pi}{a}x\right)\left(A^*_\kappa(\omega)e^{i\beta_i z} + A_\kappa(\omega)e^{-i\beta_i z}\right) \tag{1}$$

$$H_x = \frac{1}{Z(\omega)}\sin\left(\frac{\pi}{a}x\right)\left(A^*_\kappa(\omega)e^{i\beta_i z} - A_\kappa(\omega)e^{-i\beta_i z}\right) \tag{2}$$

$$H_z = -\frac{\pi}{i\omega\mu_o a}\cos\left(\frac{\pi}{a}x\right)\left(A^*_\kappa(\omega)e^{i\beta_i z} + A_\kappa(\omega)e^{-i\beta_i z}\right) \tag{3}$$

where, $Z(\omega) = \frac{\omega\mu_o}{\beta_i}$ and $\beta_i = \sqrt{k_0^2(\omega)\varepsilon_{ri} - \left(\frac{\pi}{\alpha}\right)^2}$ are the wave impedance and propagation constants and α represents the longest dimension of the finite waveguide. Also the time dependence of electromagnetic field components is assumed to be $\exp(i\omega t)$ and it is suppressed throughout the analysis. Finally an assumption taken is that the materials used are nonmagnetic ($\mu_r = 1$).

The initial aim is to calculate the transfer function of the periodic structure under investigation, shown in Fig. 2. The medium consists of $N + 1$ unit cells. The unknown variables $A_\kappa(\omega, z), A^*_\kappa(\omega, z)$ and $B_\kappa(\omega, z), B^*_\kappa(\omega, z)$ represent the complex coefficients of the reflected and transmitted waves, in layers with relative permittivities ε_{ro} and ε_{r1} respectively, for each unit cell. The thickness of the alternating layers of each unit cell are ℓ_o and ℓ_1. The $S_{21}(\omega)$ is the complex coefficient of transmission at the output of the structure. Finally, the ε_{ro} represents the relative permittivity of the air.

The analysis begins at the output of the medium, since the reflection coefficient $S_{11}(\omega)$ at the input of it ($z = 0$) is unknown for the spectrum of interest. Initially, the continuity boundary conditions are applied for the tangential electric and magnetic components, between

the interfaces of the consecutive layers of alternate dielectrics at the point $z = (N+1) \cdot \ell_1 + N \cdot \ell_o$. This is the point of the output of the periodic medium. Dividing by parts the two equations, which result from the boundary conditions, a relation arises between the reflection and transmission coefficients, in layer with relative permittivity ε_{r1} of the $N+1$ unit cell.

$$A^*_{N+1}(\omega) = \frac{\left(\dfrac{Z_o(\omega)}{Z_1(\omega)} - 1\right)}{\left(\dfrac{Z_o(\omega)}{Z_1(\omega)} + 1\right)} e^{-i2\beta_1 z} A_{N+1}(\omega) \tag{4}$$

The $Z_o(\omega)$ and $Z_1(\omega)$ represent the wave impedances of the layers with relative permittivities ε_{ro} and ε_{r1} respectively.

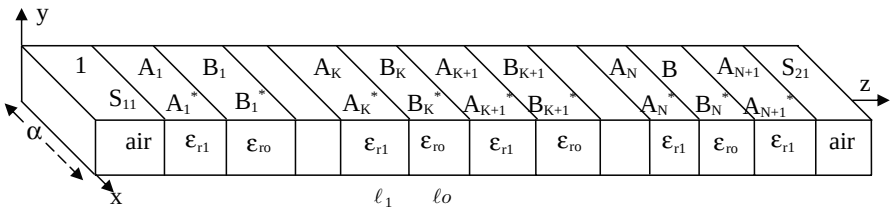

Figure 2. Loaded periodic medium without matching transformers. At each layer the reflection and transmission coefficients are presented.

Since the structure, under investigation, is a finite periodic waveguide, the analysis from the output to the input of this medium can take place in two consecutive random κ and $\kappa+1$ unit cells where $1 < \kappa < N$ (Fig. 2). Then, boundary conditions for the continuity tangential electric and magnetic components are imposed, between the interfaces of the consecutive layers at the planes of the points $z = \kappa \cdot (\ell_1 + \ell_o)$ and $z = (\kappa - 1) \cdot \ell_o + \kappa \cdot \ell_1$. Relations between the coefficients B_κ, B^*_κ and $A_{\kappa+1}, A^*_{\kappa+1}$ as well as between A_κ, A^*_κ and B_κ, B^*_κ are found. This procedure is repeated inductively up to the input of the medium. By combining the equations that arise from the continuity boundary conditions at the point $z = 0$, the following expression for the $S_{11}(\omega)$ is produced,

$$S_{11}(\omega) = \frac{Q(\omega)\left(1 + \dfrac{Z_o(\omega)}{Z_1(\omega)}\right) + 1 - \dfrac{Z_o(\omega)}{Z_1(\omega)}}{Q(\omega)\left(1 - \dfrac{Z_o(\omega)}{Z_1(\omega)}\right) + 1 + \dfrac{Z_o(\omega)}{Z_1(\omega)}} \tag{5}$$

where $Q(\omega) = \frac{A_1^*}{A_1}$.

The previous analysis shows that $A_1^* = C(z,\omega)A_{N+1}$ and $A_1 = D(z,\omega)A_{N+1}$, where $C(z,\omega)$ and $D(z,\omega)$ are complex functions. Thus, the factor $Q(\omega)$ is independent from the coefficient A_{N+1}. Since the $S_{11}(\omega)$ is known for every frequency, the previous analysis is repeated, with the input of the periodic medium as its starting point. This leads to two equivalent expressions for the $S_{21}(\omega)$,

$$S_{21}(\omega) = e^{i\beta_o z}\left(A_{N+1}^* e^{i\beta_1 z} + A_{N+1} e^{-i\beta_1 z}\right) \tag{6}$$

$$S_{21}(\omega) = e^{i\beta_o z}\left(A_{N+1} e^{-i\beta_1 z} - A_{N+1}^* e^{i\beta_1 z}\right)\left(\frac{Z_o(\omega)}{Z_1(\omega)}\right) \tag{7}$$

where $A_{N+1}^* = f(z, S_{11}(\omega))$ and $A_{N+1} = g(z, S_{11}(\omega))$.

Through the above analysis $S_{21}(\omega)$ and $S_{11}(\omega)$ coefficients and the transfer function of the finite length structure can be computed.

2.2. Analysis of the Infinite Structure

In order to understand the propagating mechanism involved in the periodic structure, it is useful to analyze the case of infinite periodicity. The infinite length periodicity solutions, which fulfill the Floquet (Bloch) theorem [6–8], provide guidance to locate highly dispersive conditions seeking to achieve strong pulse compression phenomena. The analysis deals with a periodic layered medium of infinite length, which consists of two different materials with relative permittivity $\varepsilon_r(z)$ profile given by the following expression,

$$\varepsilon_r = \begin{cases} \varepsilon_{ro}, & 0 < z < d_1 \\ \varepsilon_{r1}, & d_1 < z < d_2 \end{cases} \tag{8}$$

where d_2 is the period of a unit cell and the medium presents translational symmetry $\varepsilon_r(z) = \varepsilon_r(z + d_2)$ over the direction of propagation z.

For the same reasons with the finite structure, only the TE_{10} mode is propagate. It consists of three electromagnetic components E_y, H_x and H_z, which are equivalent with the following expressions,

$$E_y = \sin\left(\frac{\pi}{a}x\right)u(z) \tag{9}$$

$$H_x = \frac{1}{i\omega\mu_o}\sin\left(\frac{\pi}{a}x\right)\frac{\partial u(z)}{\partial z} \tag{10}$$

$$H_z = -\frac{\pi}{i\omega\mu_o\alpha}\cos\left(\frac{\pi}{a}x\right)u(z) \tag{11}$$

assuming an $\exp(i\omega t)$ time dependence. The function $u(z)$ can be found by solving the homogeneous differential wave equation of Helmholtz.

$$\left(\nabla^2 + k_0^2(\omega)\varepsilon_r\right) E_y = 0 \tag{12}$$

The $u(z)$ arises, has the following expression,

$$u(z) = c_1 \cos(\beta z) + c_2 \sin(\beta z) \tag{13}$$

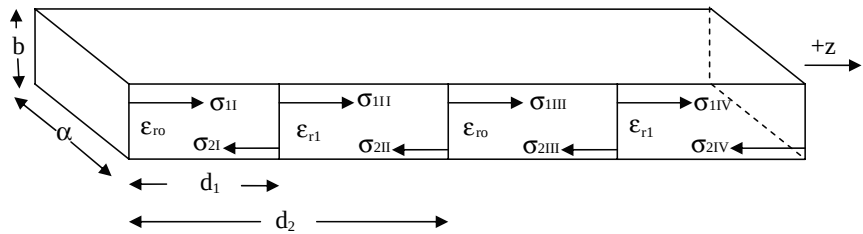

Figure 3. Two consecutive unit cells of the infinite periodic structure.

A finite part of the infinite structure, shown in Fig. 3, can be used for the analysis to take place. It consists of two unit cells, each one consisting of two layers with relative permittivities ε_{ro} and ε_{r1}. Since the medium is infinite periodic, it can be assumed that z is equal to zero, at the beginning of the selected part. By replacing the $u(z)$ with its equivalent, the tangential electric and magnetic components of the two layers of the first unit cell with relative permittivities ε_{ro} and ε_{r1}, take the following form,

$$E_{y11} = \sin\left(\frac{\pi}{a}x\right)\left(\sigma_{1I}\cos(\beta_1 z) + \sigma_{2I}\sin(\beta_1 z)\right) \tag{14}$$

$$H_{x11} = \frac{1}{i\omega\mu_o}\sin\left(\frac{\pi}{a}x\right)\left(-\beta_1\sigma_{1I}\sin(\beta_1 z) + \beta_1\sigma_{2I}\cos(\beta_1 z)\right) \tag{15}$$

$$E_{y12} = \sin\left(\frac{\pi}{a}x\right)\left(\sigma_{1II}\cos(\beta_2 z) + \sigma_{2II}\sin(\beta_2 z)\right) \tag{16}$$

$$H_{x12} = \frac{1}{i\omega\mu_o}\sin\left(\frac{\pi}{a}x\right)\left(-\beta_2\sigma_{1II}\sin(\beta_2 z) + \beta_2\sigma_{2II}\cos(\beta_2 z)\right) \tag{17}$$

The $\sigma_{1I}, \sigma_{2I}, \sigma_{1II}, \sigma_{2II}$ are the complex coefficients and β_1, β_2 the propagation constants of the layers with relative permittivities ε_{ro} and ε_{r1} respectively. Due to Block theorem, a phase factor relates the $u(z)$ and its derivative of the waves in the layer with relative permittivity ε_{ro} of the first unit cell to those of the equivalent layer of the second

unit cell.

$$\begin{pmatrix} u_3(z+d_2) \\ u_3'(z+d_2) \end{pmatrix} = e^{-i\phi} \begin{pmatrix} u_1(z) \\ u_1'(z) \end{pmatrix} \tag{18}$$

Using the relation (18) between the points $z = 0$ and $z = d_2$ and the equations derived from the continuity boundary conditions at the interfaces of the consecutive layers, at point $z = d_1$, the following eigenvalue equation gathers,

$$\begin{pmatrix} A & B \\ C & D \end{pmatrix} \begin{pmatrix} \sigma_{1II} \\ \sigma_{2II} \end{pmatrix} = e^{i\phi} \begin{pmatrix} \sigma_{1II} \\ \sigma_{2II} \end{pmatrix} \tag{19}$$

The eigenvalue of the equation is the phase factor $e^{i\phi}$. For a non-trivial solution, the following determinant must be equal to zero.

$$\begin{vmatrix} A - e^{i\phi} & B \\ C & D - e^{i\phi} \end{vmatrix} = 0 \tag{20}$$

The two reciprocal eigenvalues solutions $e^{i\phi}$, of the quadratic equation, are

$$e^{i\phi} = \frac{1}{2} \left\{ (A+D) \pm \left\{ (A+D)^2 - 4 \right\}^{\frac{1}{2}} \right\} \tag{21}$$

The solutions are reciprocal since the translational matrix (A, B, C, D) is unimodular. By replacing the terms of the equation (21) with their equivalents and solving for ϕ the following expression results,

$$\begin{aligned} \varphi \;=\; & -i \ln \left\{ \frac{1}{2} \left\{ \left(\frac{\beta_1}{\beta_2} + \frac{\beta_2}{\beta_1} \right) \sin(\beta_1 d_1) \sin(\beta_2 (d_1 - d_2)) \right. \right. \\ & + 2 \cos(\beta_1 d_1) \cos(\beta_2 (d_1 - d_2)) \\ & \pm \left(\left(\left(\frac{\beta_1}{\beta_2} + \frac{\beta_2}{\beta_1} \right) \sin(\beta_1 d_1) \sin(\beta_2 (d_1 - d_2)) \right. \right. \\ & \left. \left. \left. + 2 \cos(\beta_1 d_1)\ \cos(\beta_2 (d_1 - d_2)) \right)^2 - 4 \right)^{\frac{1}{2}} \right\} \Bigg\} \end{aligned} \tag{22}$$

3. NUMERICAL COMPUTATIONS OF PROPAGATION CHARACTERISTICS

In order to determine the dispersion properties of the proposed structure, numerical computations are carried out for the low loss alumina Al_2O_3 (ε_{r1}=9.9, $\tan(\delta)$=10^{-4}) layered structure, for both periodic and matching sections (see Fig. 1).

In order to determine pulse compression conditions, an infinite length periodic structure is initially considered, in which conditions of high dispersion are achieved. Then, using an optimization algorithm [9], the Al_2O_3 and air layers' thickness of two identical matching transformers are determined, in order to obtain minimization of the absolute reflection coefficient $|S_{11}(\omega)|$ at the input of the equivalent finite periodic structure. The two matching transformers are mirror symmetric, with respect to the mid-plane of the structure. The use of an infinite length periodic structure is very useful, since high dispersion conditions are observed even in the case of a single cell element.

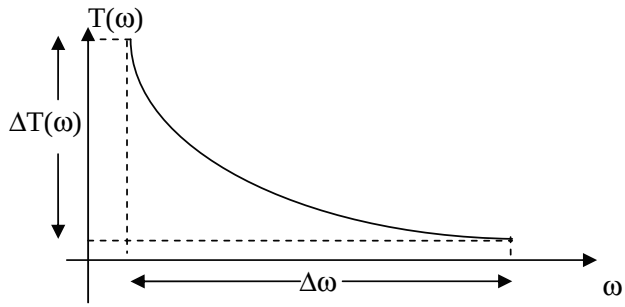

Figure 4. Presentation of physical quantities of a dispersion region.

In order to achieve pulse compression, the finite length periodic waveguide should present a transfer function, with minimum loss and phase rotation derivative (groupdelay) showing a steep and monotonic variation with respect to frequency, as indicated in Fig. 4. In this context, two physical quantities are encountered in the dispersive region:

a) the frequency bandwidth $\Delta\omega$ measured in Hz and
b) the differential time delay $\Delta T(\omega)$ measured in sec,

which are related through the expression $T(\omega) = d\varphi(\omega)/d\omega$ that associates the wave phase rotation to the group delay.

The slope of the dispersion could be positive or negative. Then the proper frequency modulation should be used in the incident wave to achieve pulse compression.

3.1. Al_2O_3 Finite Periodic Waveguide of 100 Unit Cells: Matching Transformer Based on Empirical Selection of the Layers

The first examined case is a finite periodic waveguide consisting of 100 unit cells. The unit cell has a length of 178 mm and consists

of two layers of different relative permittivities. The first involves alumina of thickness $\ell_{Al_2O_3} = 11\,\text{mm}$, and the second air of thickness $\ell_{air} = 167\,\text{mm}$. The dimensions and the relative permittivities have been chosen on the basis of the indications derived from the infinite periodic medium. The group delay $T(\omega)$, which has been computed by applying the analysis of the infinite periodic medium for 100 unit cells, is presented in Fig. 5. In this case, the area, where the $T(\omega)$ is probably capable of giving pulse compression, appears in a spectrum near 3.001 GHz, of approximately $\Delta f = 12\,\text{MHz}$, since in that bandwidth it is more intense. This case is referred to the second band pass region of the corresponding finite periodic waveguide.

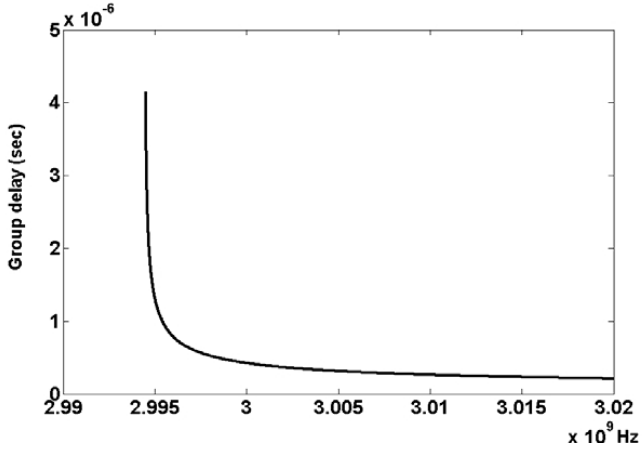

Figure 5. $T(\omega)$ derived from the analysis of the infinite periodic medium for 100 unit cells.

In Fig. 6, the corresponding absolute transmission coefficient $|S_{21}(\omega)|$ for the equivalent finite periodic waveguide is presented in the same band pass area (2.9945–3.262) GHz. As it has been expected, since there were no matching transformers used, the $|S_{21}(\omega)|$ introduces ripples, which oscillate between approximately (0.02–0.964) in the spectrum of interest. The peaks of the $|S_{21}(\omega)|$ do not reach the unity, due to the alumina losses. Finally, the number of peaks is equal to the number of unit cells of the finite periodic waveguide.

Since the area of high dispersion should have the least possible reflections, for the compression to be achieved, matching transformers should be used at the input and output of the finite periodic structure.

Initially, the matching was encountered on the basis of an empirical combination of the three air and three alumina layers' thickness, which were placed alternatively at each end of the periodic

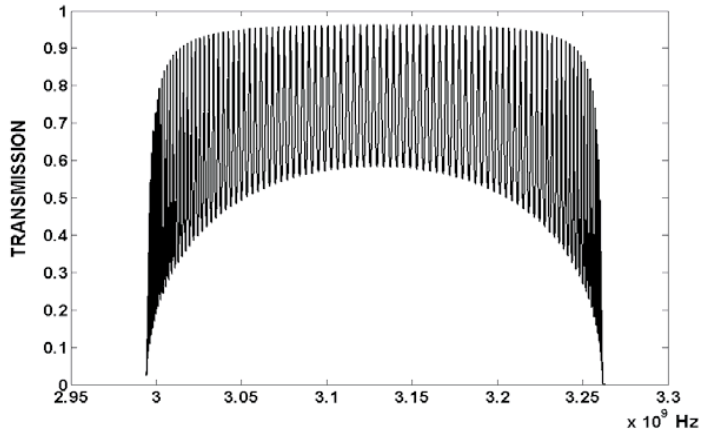

Figure 6. $|S_{21}(\omega)|$ of the finite periodic medium for 100 unit cells.

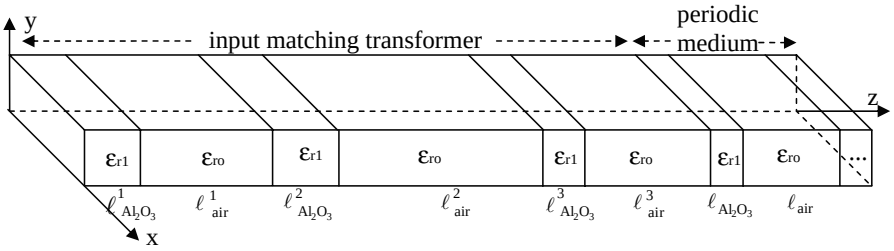

Figure 7. Input matching transformer of the finite periodic medium of 100 unit cells.

medium. In Fig. 7, the computed single transformer at the input of the structure is shown and in Table 1 the corresponding layers' thickness are presented.

The stationary wave (vswr), presented in Fig. 8, oscillates between 1–16.4. In the spectrum (2.999–3.018) GHz, where matching has been achieved, the vswr is low.

In Fig. 9, the corresponding $|S_{21}(\omega)|$ is presented. In an interval of approximately 10 MHz near 3.003 GHz, the $|S_{21}(\omega)|$ has an average value of 0.93. In the remaining spectrum, it fluctuates approximately from 0.15 to 0.96.

The calculation of the corresponding $T(\omega)$, shown in Fig. 10, is achieved by using the arithmetic method of the Taylor expansion [9]. In Fig. 10, it is confirmed that the matching transformer operates

Table 1. Al_2O_3-air transformer founded empirically, for 100 unit cells.

$\ell^1_{Al_2O_3}$	1.925 mm	ℓ^1_{air}	13.694 mm
$\ell^2_{Al_2O_3}$	9.075 mm	ℓ^2_{air}	86.673 mm
$\ell^3_{Al_2O_3}$	1.1 mm	ℓ^3_{air}	13.427 mm

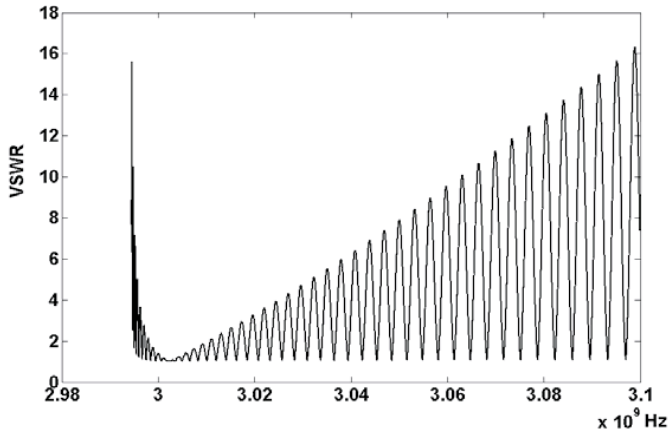

Figure 8. Stationary waves of the finite periodic medium for 100 unit cells. Its matching transformer is found by empirical selection of its layers.

well in the frequency region (2.999–3.018) GHz. In the range (3–3.004) GHz, where the transformer has its optimum performance, an average dispersion rate of $-0.023\,\mu$sec/MHz, is obtained. Therefore, it is possible for compression to be achieved in a spectrum near 3.002 GHz.

Since the $|S_{21}(\omega)|$ and $T(\omega)$ have been calculated for the mentioned matched finite structure, a Fourier analysis is carried out to examine pulse compression phenomena. In general, a stepping frequency input signal waveform is assumed for the incident wave in the finite periodic structure as follows,

$$E_{yo}\left(\frac{\alpha}{2}, 0, t\right) = \sin\left(\frac{\pi}{a}x\right) \sum_{i=1}^{M} \cos\left(\omega_i t - \beta(\omega_i) z\right) w\left(\frac{t - t_i}{w_i}\right) \qquad (23)$$

where the quantities ω_i (circular frequency), w_i (width of a pulse) and

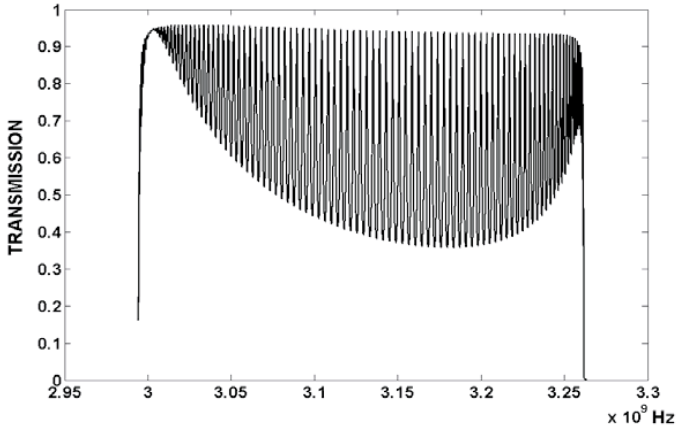

Figure 9. $|S_{21}(\omega)|$ of the finite periodic medium for 100 unit cells. Its matching transformer is found by empirical selection of its layers.

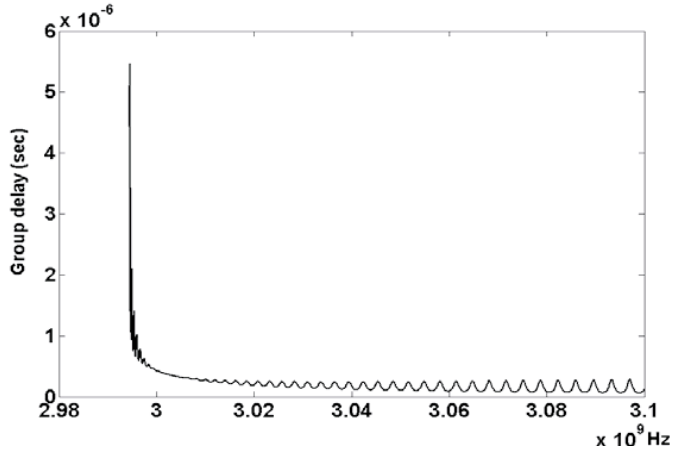

Figure 10. $T(\omega)$ of the finite periodic medium for 100 unit cells. Its matching transformer is found by empirical selection of its layers.

t_i (time beginning of a pulse) for $i = 1, 2, \ldots, M$ are defined in Fig. 11.

The output pulse waveform is computed by using the inverse Fourier transformer,

$$E_{yo}\left(\frac{\alpha}{2}, L, t\right) = \frac{1}{2\pi}\int_{-\infty}^{+\infty} \dot{S}_{21}(\omega)\dot{e}_{yo}\left(\frac{\alpha}{2}, 0, \omega\right) e^{i\omega t} d\omega \tag{24}$$

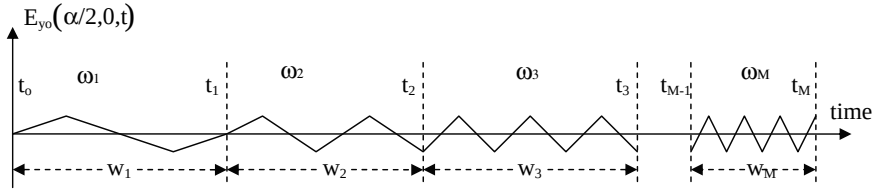

Figure 11. Stepping frequency pulse waveform.

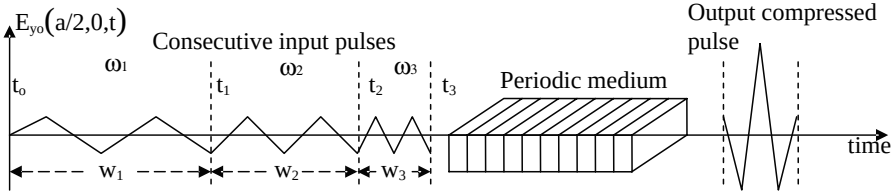

Figure 12. Stepping frequency waveform of three pulses inserted in the matched periodic medium of 100 unit cells, resulting in an output compressed pulse.

where

$$\dot{e}_{yo}\left(\frac{\alpha}{2},0,\omega\right)=\frac{1}{2\pi}\int_{0}^{t_{M-1}+w_M}E_{yo}\left(\frac{\alpha}{2},0,t\right)e^{-i\omega t}dt \tag{25}$$

is the Fourier transformer of the incident wave, L is the length of the finite structure and α the largest dimension of its orthogonal cross section.

In Fig. 13, the compression pulse at the exit of the finite periodic structure under investigation, due to a stepping frequency input signal of three pulses Fig. 12, is presented. Each pulse has a unity amplitude. The first, the second and the third pulse have respectively durations of 0.5 μsec, 0.4226 μsec, 0.16 μsec and carrier frequencies of 2.99668 GHz, 3.00252 GHz, 3.017162 GHz. The selected carrier frequencies are located in and very close to the area, where matching has been achieved. Since the output compressed pulse has approximately 1.5 amplitude, a gain of $G = 2.25$ is achieved.

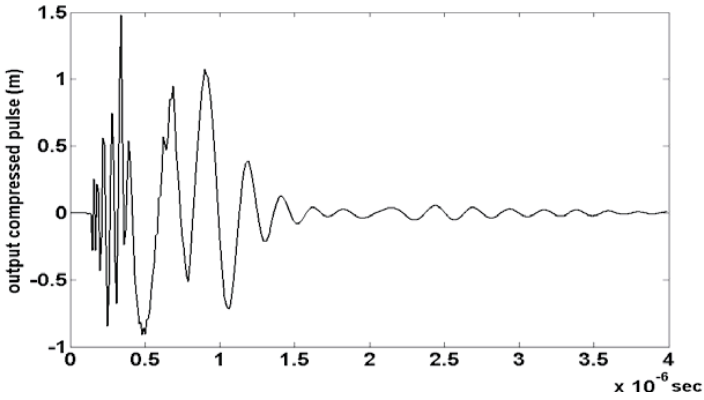

Figure 13. Computed output pulse waveform for a compressed pulse versus time.

3.2. Al_2O_3 Finite Periodic Waveguide of 100 Unit Cells: Matching Transformer Selection Based on the Powell Method

To achieve stronger phenomena of dispersion, for the same finite periodic structure the matching should be improved. Methods of optimization [9], are used to determine combinations of three alumina and three air thickness layers of the matching transformer, which will deliver optimum matching. The function to be optimized is the following,

$$G\left(\ell^1_{Al_2O_3}, \ell^2_{Al_2O_3}, \ell^3_{Al_2O_3}, \ell^1_{air}, \ell^2_{air}, \ell^3_{air}\right) = \int_{\omega_o - \frac{\Delta\omega}{2}}^{\omega_o + \frac{\Delta\omega}{2}} \left| \left| S_{11}\left(\ell^1_{Al_2O_3}, \ell^2_{Al_2O_3}, \ell^3_{Al_2O_3}, \ell^1_{air}, \ell^2_{air}, \ell^3_{air}, \omega\right)\right| - \theta \right| d\omega \quad (26)$$

The $\left|S_{11}\left(\ell^1_{Al_2O_3}, \ell^2_{Al_2O_3}, \ell^3_{Al_2O_3}, \ell^1_{air}, \ell^2_{air}, \ell^3_{air}, \omega\right)\right|$ represents the absolute value of the reflection coefficient. The constant θ is confined in the interval $0 \leq \theta \leq 1$, since the maximum possible absolute value of the reflection coefficient is 1. The constant $\Delta\omega$ represents the spectrum of frequencies, at which matching has to be achieved. The independent variables of the function G represent the thickness of the layers of the matching transformer.

Once a local minimum is found, the corresponding combination of the $\ell^1_{Al_2O_3}, \ell^2_{Al_2O_3}, \ell^3_{Al_2O_3}, \ell^1_{air}, \ell^2_{air}, \ell^3_{air}$ is given, so that the absolute

reflection coefficient in the spectrum $\Delta\omega$ is almost equal to θ. Powell arithmetic method [9] is used for optimization.

Since there are restrictions in the independent variables, penalty functions are used solving the problem of minimization in the area of interest. In our case, the independent variables are greater or equal to zero, since they represent length. Also they are less or equal to 0.1 m, so that the reflection coefficient achieved corresponds to a structure that has practical meaning. The penalty function and the penalty term, mentioned in [10], are given by the following expressions,

$$q(\mu, \vec{x}) = G(\vec{x}) + \mu P \tag{27}$$

and

$$P = \sum_{\kappa=1}^{6} \left[\left(\min \{0, g_{2\kappa-1}(y_\kappa)\} \right)^2 + \left(\min \{0, g_{2\kappa}(y_\kappa)\} \right)^2 \right] \tag{28}$$

respectively, with $\vec{x} = \left(\ell^1_{Al_2O_3}, \ell^2_{Al_2O_3}, \ell^3_{Al_2O_3}, \ell^1_{air}, \ell^2_{air}, \ell^3_{air} \right)$, μ a non-negative term and $y_\kappa = \ell^\kappa_{Al_2O_3}$, for $\kappa = 1, 2, 3$ and $y_\kappa = \ell^{\kappa-3}_{air}$ for $\kappa = 4, 5, 6$. The space at which the local minima are determined, is $F = \left\{ \vec{x} \in IR^6 : g_j(y_\kappa) \geq 0 \forall j \forall \kappa,\ j = 1, \ldots, 12,\ \kappa = 1, \ldots, 6 \right\}$ where,

$$g_j(y_\kappa) = \begin{cases} 0.1 - y_\kappa & j = 2\kappa \\ y_\kappa & j = 2\kappa - 1 \end{cases} \tag{29}$$

represent the conditions of restriction. Therefore, when the components of $\vec{x}$, corresponding to the $\min\limits_{\vec{x} \in IR} \{q(\mu, \vec{x})\}$ of a local valley, do not satisfy the conditions of restriction, the $P \neq 0$. Then, μ is selected so that, the $q(\mu, \vec{x})$ can be shifted to a new valley of a local minima. The non-limited problem is solved again, until the components of $\vec{x}$, corresponding to a local minima, satisfy the conditions of restriction.

A combination of thickness $\ell^1_{Al_2O_3}, \ell^2_{Al_2O_3}, \ell^3_{Al_2O_3}, \ell^1_{air}, \ell^2_{air}, \ell^3_{air}$, giving a satisfactory $|S_{21}(\omega)|$, is determined, based on the above mentioned analysis. The layers' (Table 2) are positioned at the input of the structure, in the same order, as in Fig. 7.

In Fig. 14 the vswr is presented. In the spectrum (2.9945–2.999) GHz where matching is weak and dispersion is the strongest, the vswr is high and oscillates from 1 to 14.1. In the remaining spectrum, where good matching is achieved the vswr fluctuates between 1–1.8.

The $|S_{21}(\omega)|$, represented in Fig. 15, fluctuates between 0.16–0.91 in the bandwidth (2.9945–2.999) GHz, since in that area the reflected power and the losses are great due to mismatch and to high

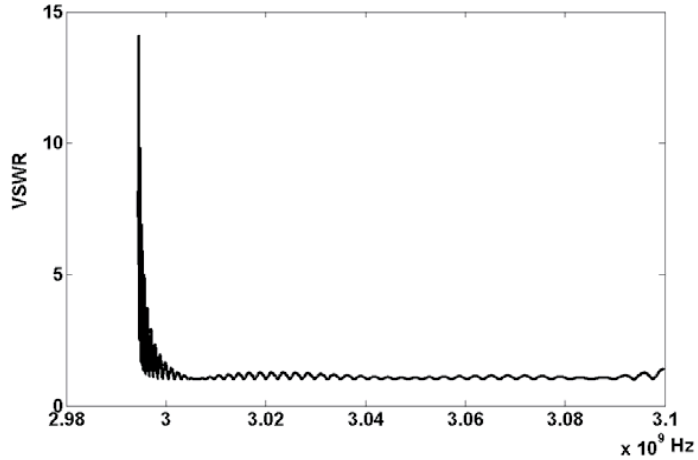

Figure 14. Stationary waves of the finite periodic medium for 100 unit cells. Its matching transformer is found by using Powell method.

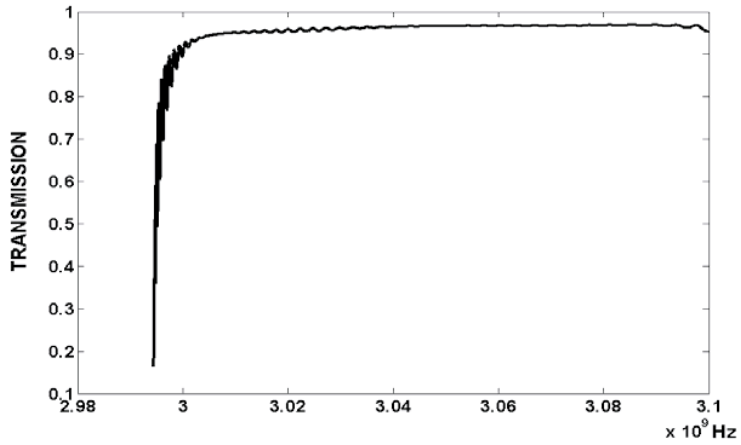

Figure 15. $|S_{21}(\omega)|$ of the finite periodic medium for 100 unit cells with matching transformer calculated with the help of Powell method.

Table 2. Al_2O_3-air transformer founded with the help of Powel method for 100 unit cells.

$\ell^1_{Al_2O_3}$	47.3 mm	ℓ^1_{air}	96.7 mm
$\ell^2_{Al_2O_3}$	18.5 mm	ℓ^2_{air}	66.3 mm
$\ell^3_{Al_2O_3}$	67.1 mm	ℓ^3_{air}	51.7 mm

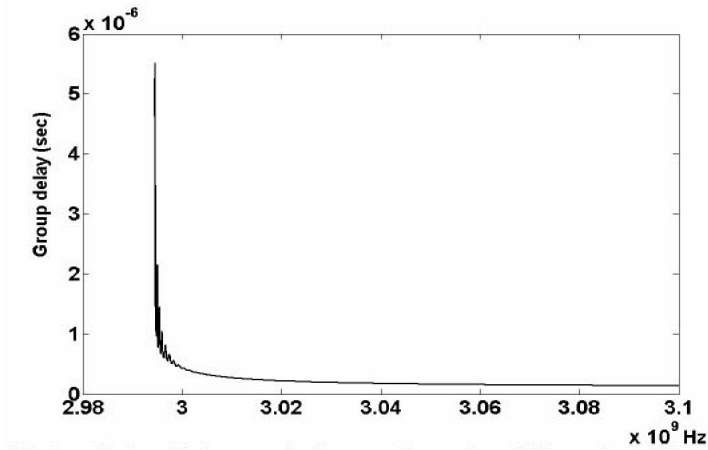

Figure 16. $T(\omega)$ of the finite periodic medium for 100 unit cells with matching transformer, calculated with the help of Powell method.

vswr respectively. In the remaining spectrum the ripples have almost disappeared and the $|S_{21}(\omega)|$ has an average value of 0.93.

The $T(\omega)$ in Fig. 16 is smoother than in the previous case, except in the cut off region where the matching is weak. Strong dispersion is achieved at the frequency regions (3.0017–3.0027) GHz, (3.0027–3.0047) GHz and (3.0047–3.0127) GHz with average rates of -0.0278 μsec/MHz, -0.0171 μsec/MHz and -0.0095 μsec/MHz, respectively.

3.3. Al_2O_3 Finite Periodic Waveguide of 645 Unit Cells with Matching Transformer Calculated with the Help of Powell Method

The next step is to find other Al_2O_3 periodic structures of stronger compression phenomena. This can be achieved by applying the Powell method in the transfer function of a single unit cell of the

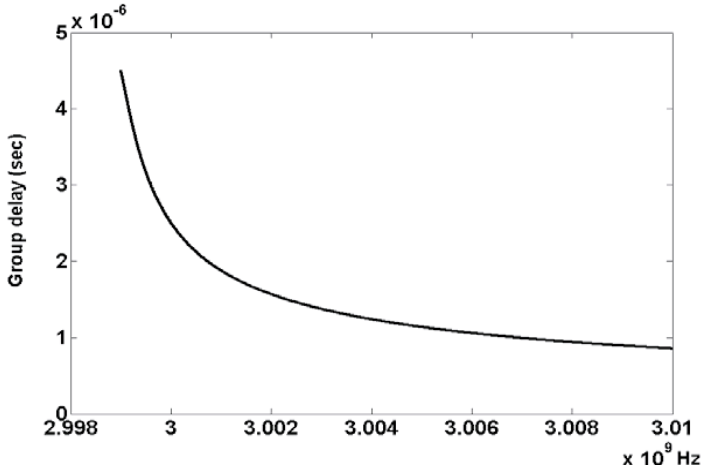

Figure 17. $T(\omega)$ of the infinite periodic structure is presented for 645 unit cells.

Table 3. Al_2O_3-air transformer founded with the help of Powel method for 645 unit cells.

$\ell^1_{Al_2O_3}$	25.5 mm	ℓ^1_{air}	64.8 mm
$\ell^2_{Al_2O_3}$	21.1 mm	ℓ^2_{air}	75.3 mm
$\ell^3_{Al_2O_3}$	70.43 mm	ℓ^3_{air}	38.9 mm

infinite periodic medium, so that its layers' thickness providing strong phenomena of dispersion, can be determined.

In Fig. 17, the $T(\omega)$ of the infinite periodic medium is presented, corresponding to an equivalent finite periodic structure of 20 m. Each unit cell consists of an Al_2O_3 and air layers of thickness $\ell_{Al_3O_2} = 15$ mm and $\ell_{air} = 16$ mm, respectively. The structure consists of 645 unit cells. Using again the Powell method and penalty functions, the thickness combination of the finite structure transformer presented in Table 3, is determined. The transformer results in a matching for a bandwidth of 11 MHz. Also in this example, the layers' are positioned in the same order as in Fig. 7, at the input of the structure.

The $|S_{21}(\omega)|$, presented in Fig. 18, fluctuates from 0.0003–0.2724. It is too low, since the total Al203 thickness of the finite structure is 9.91 m, in contrast to the previous cases where 1.1242 m and 1.3658 m

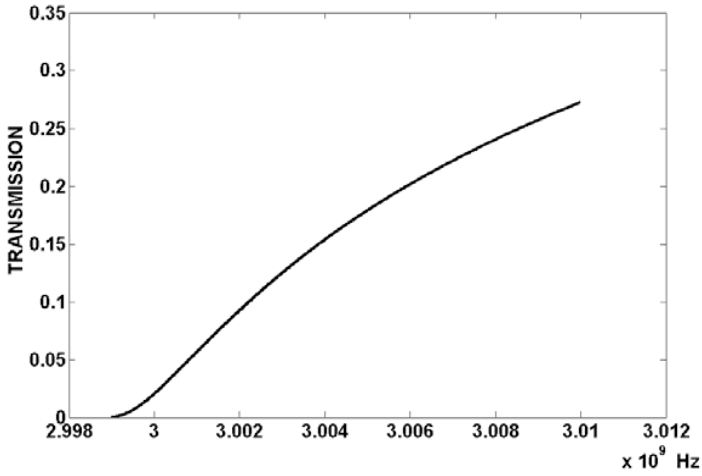

Figure 18. $|S_{21}(\omega)|$ of the finite periodic medium for 645 unit cells with matching transformer, calculated with the help of Powell method.

are used.

The vswr, shown in Fig. 19, fluctuates between 1.05–3.9. It is high near the cut off area where the dispersion is stronger. However, in this area it is much less higher compared to the examples that have already been mentioned, since the matching is much better. This is the reason why the $|S_{21}(\omega)|$ is smoother in that case.

The $T(\omega)$, shown in Fig. 20, presents strong average dispersion rate of $-1.872\,\mu$sec/MHz, $-0.4665\,\mu$sec/MHz and $-0.09\,\mu$sec/MHz corresponding to the frequency regions (2.999–3) GHz, (3–3.002) GHz and (3.002–3.01) GHz. In comparison with the previous cases is smoother without ripples, wider and presents stronger phenomena of dispersion, in a spectrum of 11 MHz.

In conclusion, since the percentage of the propagating power is low, the compression likely to be achieved may be of no use,

3.4. TiO_2 Finite Periodic Waveguide of 1695 Unit Cells with Matching Transformer Calculated with the Help of Powell Method

In the effort to find stronger compression phenomena, a dispersive medium of a low loss material, titanium dioxide TiO_2 ($\varepsilon_{r1} = 25$, $\tan(\delta) = 4 * 10^{-5}$) is used instead of Al_2O_3. With the help of Powell method, applied in an infinite length periodic medium, a finite

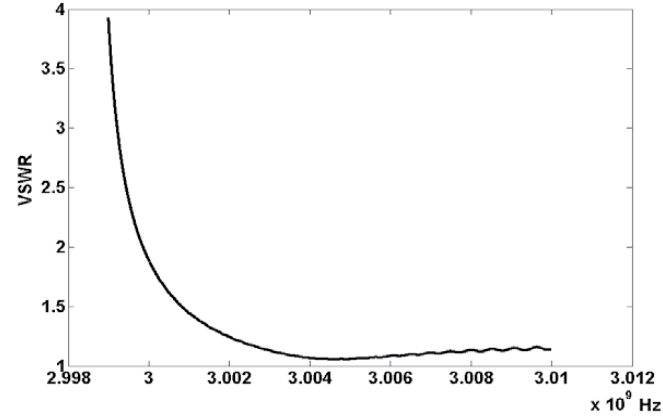

Figure 19. Stationary waves of the finite periodic medium for 645 unit cells with matching transformer, calculated with the help of Powell method.

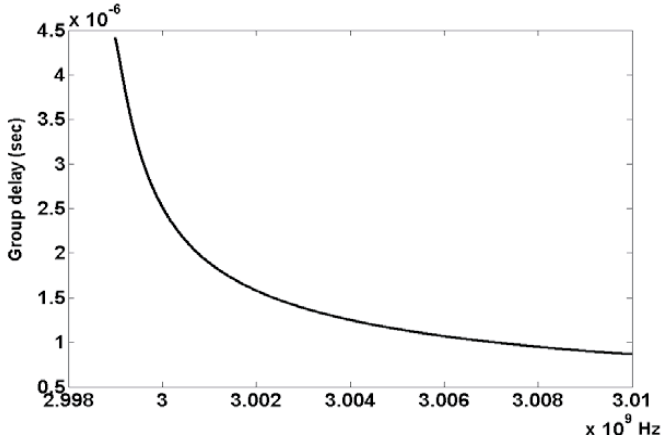

Figure 20. $T(\omega)$ of the finite periodic medium for 645 unit cells with matching transformer, calculated with the help of Powell method.

structure was found with its unit cell, consisting of an air and a TiO_2 layers of $\ell_{\text{air}} = 7.2\,\text{mm}$ and $\ell_{TiO_2} = 4.6\,\text{mm}$ thickness, respectively. The equivalent finite periodic structure consists of 1695 unit cells and has a length of 20 m.

Using again the Powell method and penalty functions, in order matching to be achieved, the combination of Table 4 of three TiO_2 and three air layers' thickness was found. And in this case, the layers'

Table 4. Table 4. TiO_2-air transformer founded with the help of Powel method for 1695 unit cells.

$\ell^1_{TiO_2}$	64.3 mm	ℓ^1_{air}	63.2 mm
$\ell^2_{TiO_2}$	24.6 mm	ℓ^2_{air}	30.2 mm
$\ell^3_{TiO_2}$	15.6 mm	ℓ^3_{air}	64.5 mm

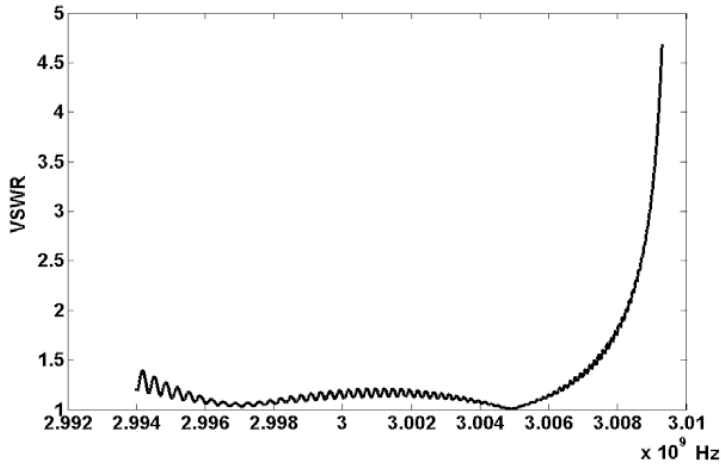

Figure 21. Stationary waves of the finite periodic medium for 1695 unit cells of TiO_2 with matching transformer, calculated with the help of Powell method.

are positioned at the input of the structure in the same order as in Fig. 7.

In Figures 21, 22, and 23, the vswr, the $|S_{21}(\omega)|$ and the corresponding $T(\omega)$ are presented. In this case, the $T(\omega)$ has a positive inclination, it has no ripples and compared with the previous cases, it has the highest maximum value of approximately 11 μsec. Phenomena of high dispersion appear in frequency regions (2.9983–3.0063) GHz, (3.0063–3.0083) GHz and (3.0083–3.0093) GHz with average rates of 0.1825 μsec/MHz, 0.9741 μsec/MHz and 5.6915 μsec/MHz, respectively.

For the same bandwidths the vswr oscillates between 1–4.7 and the $|S_{21}(\omega)|$ between 0.01–0.53, respectively. The $|S_{21}(\omega)|$ is very low again, especially at the region where the phenomenon of dispersion is

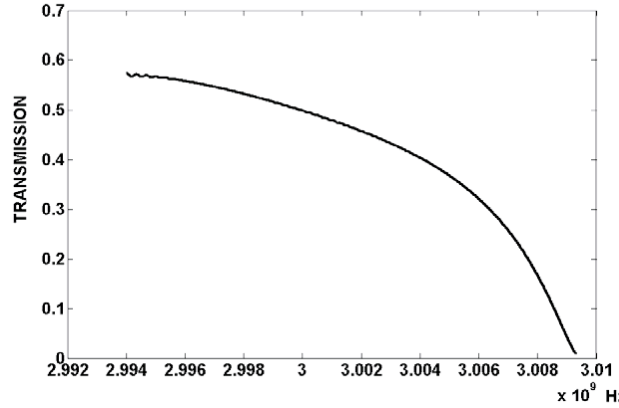

Figure 22. $|S_{21}(\omega)|$ of the finite periodic medium for 1695 unit cells of TiO_2 with matching transformer, calculated with the help of Powell method.

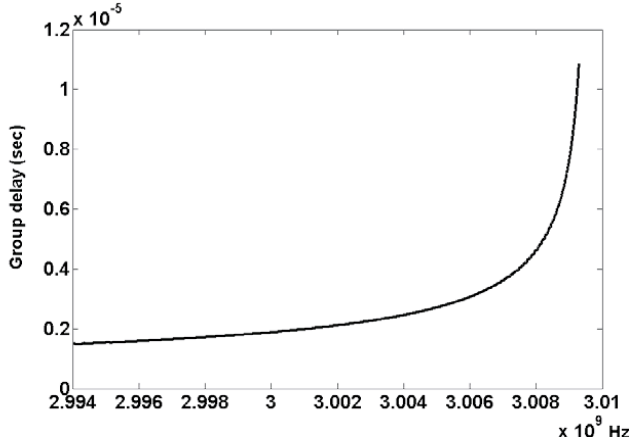

Figure 23. $T(\omega)$ of the finite periodic medium for 1695 unit cells of TiO_2 with matching transformer, calculated with the help of Powell method.

strong, since the thickness of TiO_2 used is 7.9 m. Therefore, also in that case the compression to be possibly achieved, is probably of no use.

The next step is to carry out, experimentally, the example of Section 3.2, since it is the only periodic medium that has practical meaning. As the construction of 100 unit cells is of high cost, a periodic medium of 14 unit cells was built. In Fig. 24, the corresponding

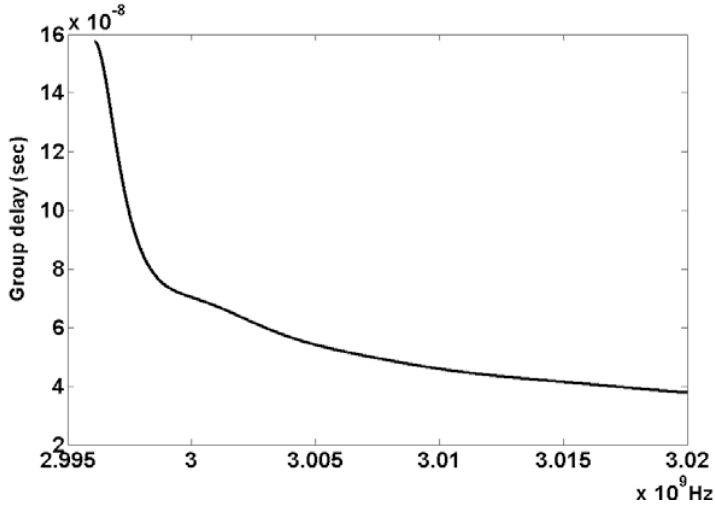

Figure 24. $T(\omega)$ of a finite periodic medium of 14 unit cells with matching transformer calculated with the help of Powell method

simulation of the $T(\omega)$ with the highest value of 156 nsec is presented.

Strong phenomena of dispersion appear in the frequency regions (2.9961–2.9971) GHz, (2.9971–2.9991) GHz and (2.9991–3.0071) GHz with average rates of $-0.042\,\mu$sec/MHz, $-0.021\,\mu$sec/MHz and $-0.003\,\mu$sec/MHz, respectively.

3.5. Comparison of the Transmission Coefficients in the Cases of the Matched Periodic Mediums of 14 Unit Cells, with and without Metallic Envelope

Up to now, the losses due to the metallic envelope of the waveguide are not included in the results. The attenuation of the propagating waves [11] can be found from,

$$a_p = \frac{A_p}{2} \tag{30}$$

with A_p, representing the percentage of losses per unit length in the direction of propagation z, due to the metallic envelope. It is expressed as the ratio of the power losses in the perimeter P_a(W/m) of the waveguide towards the total power P_σ inserted. In case that only

the TE_{10} mode propagates, the expression of A_p is,

$$A_p = \frac{P_a}{P_\sigma} = \frac{2\left(1 + \frac{2b}{a}\left(\frac{f_{10}}{f}\right)^2\right)}{Z\sigma\delta_s b\left(1 - \left(\frac{f_{10}}{f}\right)^2\right)^{1/2}} \tag{31}$$

where

$$\delta_s = \left(\frac{1}{\pi f \mu_o \sigma}\right)^{1/2} \tag{32}$$

with $\sigma = 5.8 * 10^7$ the conductivity of copper, $Z = 120\pi$ the wave impedance in the air, $f_{10} = 1.736\,\text{GHz}$ the cut off frequency of the TE_{10} mode and a, b the dimensions of the orthogonal cross section of the waveguide of type WR-340.

In Fig. 25 the $|S_{21}(\omega)|$ is presented for both cases in a bandwidth of 100 MHz. The solid line graph presents the situation without losses and the dot line one with losses. Comparing the two graphs, it is observed that the power propagated through the finite matched periodic medium of 14 unit cells, for both situations, is almost the same.

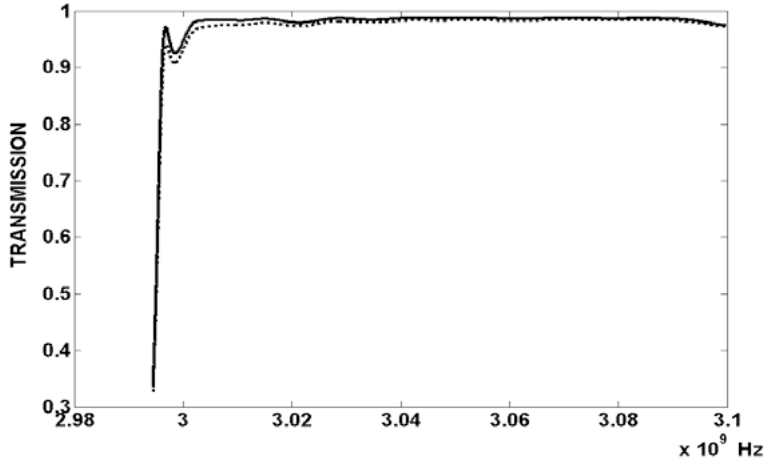

Figure 25. $|S_{21}(\omega)|$ of a finite periodic medium of 14 unit cells with and without the metallic envelope.

4. EXPERIMENTAL STUDY OF THE FINITE PERIODIC WAVEGUIDE OF 14 UNIT CELLS

The final step of the survey is the comparison of theoretical and experimental results and their similarity. In the structure that is analyzed, the layers of alumina Al_2O_3 are almost impossible to be placed with accuracy at the coordinates that have been calculated by the theoretical analysis. For this reason, a material of stable form, the doou, is used instead of the air, which has relative permittivity of approximately 1.18, at the spectrum of interest.

The experimental structure, is a periodic waveguide medium of 14 unit cells without matching transformers at its input and output. At the ends of it, short-circuited waveguides of a much smaller length, are placed. In each of them, a unipolar antenna has been placed at a distance $(\lambda/4)$ m from the short-circuit side. The wavelength λ corresponds in the central frequency of the spectrum of interest. The antenna ends are connected to a male N-type connector. Via the N-type connectors the structure is connected to the network analyzer HP8718D. By using the network analyzer, the S-parameters are calculated with the help of the TRL (Through Reflection Line) method.

In Fig. 26, the parameters S_{11} (solid line) and S_{21} (dot line) in dB are presented. As it can be observed, the band pass region has been shifted by approximately 42.1MHz compare with the theoretical one, in the cut off frequency area near 2.956 GHz. The displacement

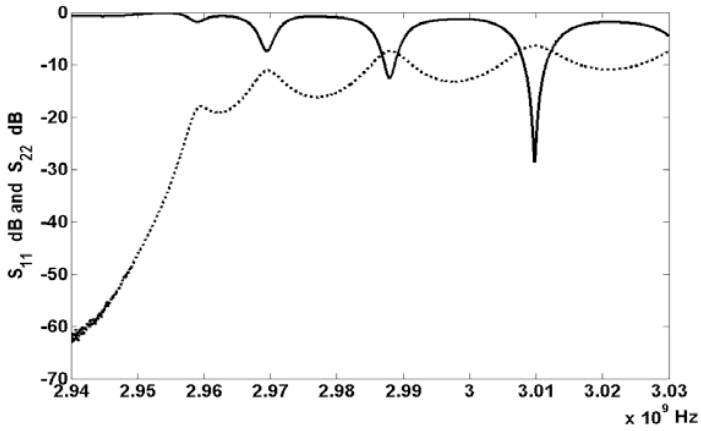

Figure 26. S_{11} (solid line) and S_{21} (dot line) in dB for the periodic waveguide of 14 unit cells without matching transformer.

in the spectrum is due to the fact that the thickness of the layers of Al_2O_3 and of doou is not identical to the ones calculated in the theory. Also, the real and imaginary parts of their relative permittivities differ from the ones assumed in the simulations. Another assumption taken in the simulations is that the assumed layers of the materials were identical. It is not known however, whether the method used for the construction of the alumina layers in the experimental structure was recursive. Furthermore, as the construction of the alumina layers is very difficult, the produced ones have not uniformed interfaces perpendicular to the direction of propagation. The dissimilarities of the alumina layers oscillate between 0.2 mm–0.5 mm and these of the doou between 0.01 mm–0.1 mm. Finally, the Al_2O_3 layers do not fit completely inside the waveguide. During their position, they are damaged and a small number of them is not placed perpendicular to the direction of propagation. The particular method is of high sensitivity and requires high accuracy for the dimension parameters to the level of 10^{-4}–10^{-5} m.

In Fig. 27, the power losses of the propagating waves through the finite periodic waveguide are presented. The losses in some spectrums of the band pass area, fluctuate between 14.5%–27% and in some others they oscillate from 74%–77%. They are mainly due to the imaginary part of the Al_2O_3. This has been expected, since the losses of a material depend on its crystal structure. Thus, for the achievement of the needed losses, a suitable elaboration is required, which is very expensive. Finally, some losses appeared at the band stop spectrum.

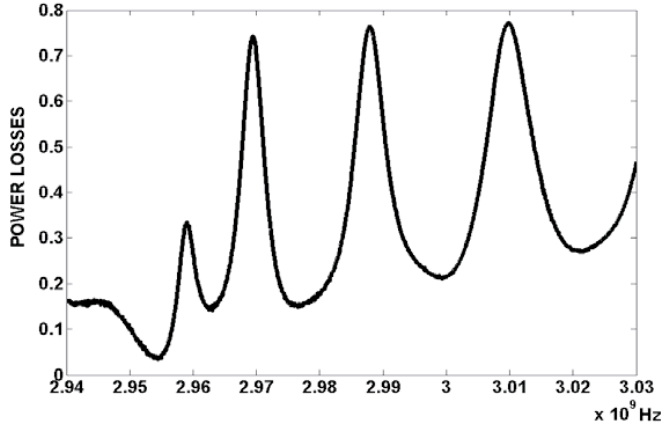

Figure 27. Power losses of the propagating waves through the finite periodic waveguide of 14 unit cells without matching transformer.

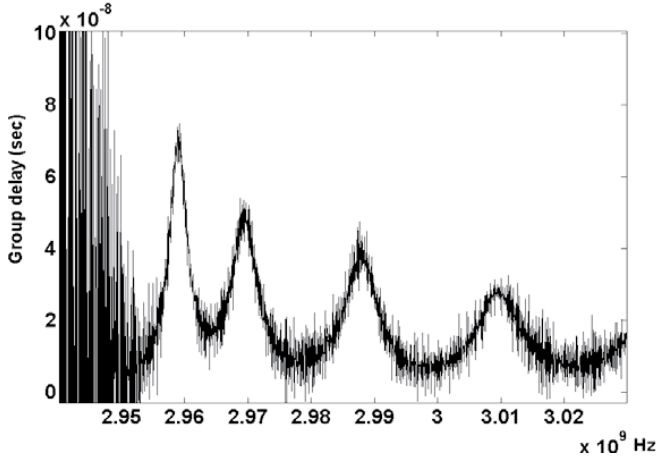

Figure 28. $T(\omega)$ for the finite periodic structure of 14 unit cells without matching transformer.

This false result is due to calibration problems in the TRL method.

The $T(\omega)$ is shown in Fig. 28. Since matching transformers are not used, it does not decline smoothly from the frequency 2.959 GHz to 3.0212 GHz. Between these values of spectrum, a number of local maxima are interpolated in areas near the frequencies 2.959 GHz, 2.9695 GHz, 2.988 GHz and 3.0095 GHz. Their corresponding $T(\omega)$ values are approximately 71.1 nsec, 51.4 nsec, 43.4 nsec and 29 nsec. Also local minima are interpolated in areas near the frequencies 2.9639 GHz, 2.9781 GHz, 2.9989 GHz and 3.0212 GHz, corresponding approximately to $T(\omega)$ values of 8 nsec, 7 nsec, 10 nsec and 5 nsec. Therefore, it is clear that the $T(\omega)$ of the experimental structure deviates from the one derived from the simulation. The frequency regions, that reveal a weak phenomenon of dispersion and are presented in areas of negative slope, near the local maxima, are (2.9591–2.9639) GHz, (2.9696–2.9748) GHz, (2.9882–2.995) GHz and (3.0095–3.0155) GHz. Their corresponding average dispersion rates are $-0.0125\,\mu$sec/MHz, $-0.0081\,\mu$sec/MHz, $-0.0039\,\mu$sec/MHz and $-0.0031\,\mu$sec/MHz.

A matching transformer has been built, but it was not used because its experimental dimensions did not coincide with the theoretical ones and therefore, no matching could be achieved. Finally, the experimental structure is not periodic since the thickness of the layers is not the same for every unit cell due to construction accuracy problems.

Completing the examination of the characteristics of the experimental structure, it is in question whether it is capable of providing compression. In Fig. 28 there are four areas of relative high dispersion. Therefore, a number of them will be used, so that compression can be achieved. In the next example, three pulses are transmitted consecutively in the following order, with carrier frequencies 2.961 GHz, 2.972 GHz, 2.994 GHz and with duration of 230 nsec. The order has been chosen so that the carrier frequencies, which correspond to high $T(\omega)$, propagate through the medium first, and the ones with smaller $T(\omega)$ follow. The carrier frequencies of the pulses have been selected so that compression can arise.

In Fig. 29 the time interval, corresponding to the horizontal side of a single box, is 100 nsec. Also, the amplitude intervals, which correspond in the perpendicular side of a single box, are 200 mV and 20 mV, for the top and the bottom graphs respectively. Finally, their dc levels differ by approximately 1150 mV, which confirms that the losses of the propagating wave through the dispersive medium are high.

The time position of the compression achieved is shown at the bottom of the graph of Fig. 29. At the top of the graph of Fig. 29, the corresponding time positions of the sinusoidal pulses are shown. The output compressed pulse, is originated, mainly, from the first two sinusoidal pulses and its absolute amplitude is 119 mV. An unwanted pulse appears between the second and the fourth pulse in Fig. 29. Its appearance is due to source constraints.

The arrangement of Fig. 30 provides the results of Fig. 29. It consists of a source of two ports, with each port producing consecutive sinusoidal pulses of the same duration but of different frequency.

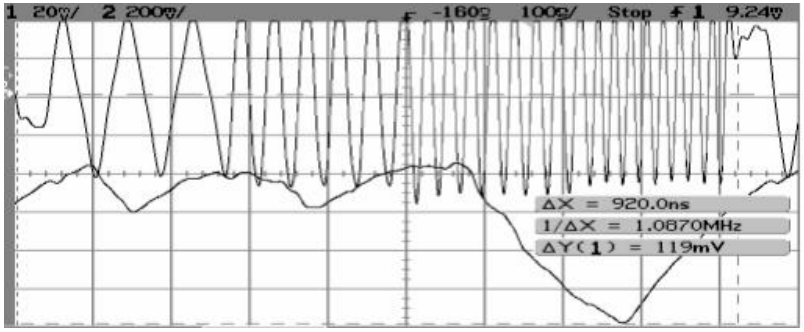

Figure 29. Time positions of the output compressed pulse and of the consecutive sinusoidal pulses inserted in the periodic medium, presented at the bottom and the top graphs respectively.

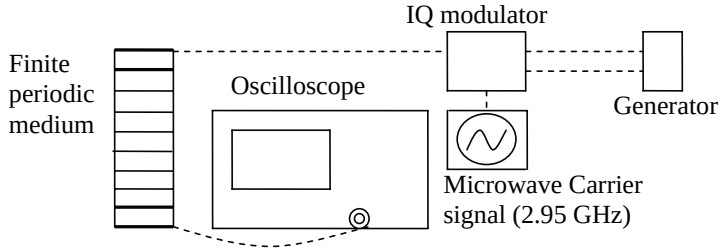

Figure 30. This arrangement provides the results of Figure 29.

The signals between the two ports have a 90^o phase difference and their frequencies are digitally controlled. Limitations of the source capabilities, are that the durations of the consecutive pulses, must be the same and their frequencies must differ by a constant amount. The signals, in their turn, are inserted in an IQ modulator, which is connected to a generator operating in 2.95 GHz. The modulator, initially, shifts the spectrum, corresponding to the pulses originated from the source, to the microwave carrier frequency and in succession, it suppresses the left sideband region and the carrier frequency of the derived signal. Finally, the single sideband signal is inserted in the periodic structure and its output is ejected in an oscilloscope.

5. CONCLUSION

A finite length dielectric loaded rectangular cross section metallic wall, exhibiting phenomena of dispersion, has been studied theoretically and experimentally, aiming at the achievement of pulse compression. Equivalent infinite periodic structures have been used, since, in that case, high dispersion conditions can be found even in a single element. An infinite structure gives a very good approximation of intensity, steepness as well as of the position of a dispersion phenomenon in the spectrum, of the equivalent finite structure.

The stronger, the wider and the smoother the phenomenon of dispersion of a structure is, the higher the power losses are, since the quantity of the Al_2O_3 and of the TiO_2 used is greater. Therefore, there is a balance between the transmission coefficient and the characteristics of dispersion of the finite periodic structure.

Furthermore, a comparison is carried out of the dispersion characteristics between finite periodic structures of the same length, containing high quantity of Al_2O_3 in one case and TiO_2 in the other, in equal intervals of frequencies. The above comparison has shown that the smaller the $\tan(\delta)$ and the higher the real part of the dielectric is,

the more intense and steep the group delay versus ω is.

Having taken into consideration the simulation and the experimental results regarding the finite periodic structures, it is concluded that the pulse compression capability is weakened. This is due to the magnitude and shape of dispersion, which is not able to cause strong compression for the stepping frequency input signals of three sinusoidal pulses mentioned in Sections 3.1 and 4.

In practice, this kind of transfer function and incident wave Fourier transformer are required, so that the inverse Fourier transformer of their product, presenting the output compressed pulse, can be as strong as possible, in the smallest possible time interval.

It should be underlined that, the particular method is of high sensitivity and requires high accuracy for the dimension parameters, so that the theoretical and the experimental characteristics can coincide. This is confirmed, by the displacement of the cut off frequency of the second band pass area in the experimental structure, in relation to the cut off one of the theoretical structure of 14 unit cells.

REFERENCES

1. Tantawi, S. G., R. D. Ruth, A. E. Vlieks, and M. Zolotorev, "Active high-power RF pulse compression using optically switched resonant delay lines," *IEEE Transactions on Microwave Theory and Techniques,* Vol. 45, No. 8, 1486–1492, August 1997.
2. Wilson, P. B., Z. D. Farkas, and R. D. Ruth, "SLED II: a new method of RF pulse compression," presented at the *Linear Accl. Conf.,* Albuquerque, NM, Sept. 1990.
3. Farkas, Z. D., "Binary peak power multiplier and its application to linear accelerator design," *IEEE Trans. Microwave Theory Tech.,* Vol. MTT-34, 1036–1043, Oct. 1986.
4. Stout, B., S. Stout, and M. Nevière, "Photonic crystal waveguides: a one-dimensional model theory," *Journal of Electromagnetic Waves and Applications*, Vol. 15, No. 7, 961–988, 2001.
5. Hillion, P., "Electromagnetic pulse propagation in dispersive media," *Progress In Electromagnetics Research*, PIER 35, 299–314, 2002.
6. Yeh, P., A. Yariv, and C.-S. Hong, "Electromagnetic propagation in periodic stratified media. I. General theory," *J. Opt. Soc. Am.* Vol. 67, 423–437, 1977.
7. Wu, L., S. He, and L. Shen, "Band structure for a one-dimensional photonic crystal containing left-handed materials," *Physical Review B,* Vol. 67, No. 235103, 1–6, 2003.

8. Magnus, W. and S. Winkler, *Hill's Equation,* Dover Publications Inc., New York, 1979.
9. Press, W., S. Teukolsky, W. Vetterling, and B. Flannery, *Numerical Recipes in Fortran,* Cambridge University Press, 1992.
10. Fletcher, R., *Practical Methods of Optimization,* John Wiley and Sons Ltd, 1987.
11. Marcuvitz, N., *Waveguide Handbook,* New York Dover Publications, Inc., 1951.

Efstratios C. Thirios received his degree in B.Eng. (Hons) in Electronic Engineering from Queen Mary and Westfield College of University of London in 1999 and his Master of Science degree in Microwaves and Optoelectronics from University College London (UCL) of University of London in 2000. He is currently working toward the Ph.D. degree in the department of Electrical and Computer Engineering of the National Technical University of Athens (NTUA). He has an accepted paper in journal and an accepted article in Conference and his current research interest is the study of pulse compression phenomena in the microwave frequency region, through passive structures.

Dimitra I. Kaklamani was born in Athens, Greece, in 1965. In 1982, she entered the National Technical University of Athens (NTUA), Department of Electrical Engineering, from where she graduated in 1987, receiving the Diploma degree in Electrical Engineering. In August 1992, she received the Ph.D. degree from NTUA in Electrical and Computer Engineering. During the years 1993–1996, she was a research associate at the Institute of Communications and Computer Systems (ICCS), in NTUA, participating in several European Union and National projects in telecommunications. From January 1994, until September 1996, she worked as a consultant in microwave networks design at the Hellenic Telecommunications Organization SA. In April 1995 and, April 2000, she was elected Lecturer and Assistant Professor respectively at NTUA, Department of Electrical and Computer Engineering. Dr. Kaklamani has over 120 publications in the fields of software development for information transmission systems modeling, microwave networks, mobile and satellite communications. She has co-ordinated the ICCS and NTUA activities in the framework of several European Union and National projects in the same areas and has been a national representative for EU/COST actions in electromagnetic compatibility and smart antennas. She is a reviewer for the Hellenic General Secretariat for

Research and Technology, reviewer for several IEEE journals and editor of the international book *Applied Computational Electromagnetics: State of the Art and Future Trends* (Springer-Verlag, New York, 2000). Dr. Kaklamani has been member of the Program Committee, reviewer and invited lecturer for several international Conferences and has been invited to join the Electromagnetics Academy as a distinguished member. Her current research interests focus on the use of object oriented methodologies and middleware technologies for the development of distributed systems, as well as development of visualization and real time simulation techniques for solving complex large-scale modeling problems of microwave engineering and information transmission systems. Dr. Kaklamani is a member of IEEE and the Technical Chamber of Greece.

Nikolaos K. Uzunoglu is a Professor of the School of Electrical and Computer Engineering (SECE) at National Technical University of Athens (NTUA) from 1987. He holds a Degree in Electrical and Computer Engineering from Polytechnic University of Instanbul (1973), a M.Sc. in Quantum Electronics (1974) and a Ph.D. in Microwaves ("Theoretical calculations of scattering of electromagnetic waves from precipitation particles") (1976) from University of Essex and a postdoc at NTUA (1982). He has served as President of SECE for 6 years (1986–1992) and as Director of the Institute of Communications and Computer Systems/NTUA from 1992–1999. He is the Head and the Technical Manager of Microwave and Fiber Optics Lab while he has been the Scientific Co-ordinator in more than 100 national and European programs. His research interests are in the field of microwave and fiber optics telecommunications, wireless telecommunications, radar systems and remote sensing, applications of electromagnetic theory and biomedical engineering, microwave and field measurements. He has published over 200 papers and articles in Conference Proceedings with evaluation process and International Journals, 3 scientific books and more than 200 technical reports. He was given the International G. Markoni award in 1981 and he is a Member of IEEE, of the Technical Chamber of Greece and National Representative for the European Union Cost Telecommunications programs.